EFFICIENT STRESS AND FAILURE ANALYSIS OF BOLTED JOINTS FOR COMPOSITE LAMINATES

M. Nguyen-Hoang, W. Becker
Fachgebiet Strukturmechanik
Technische Universität Darmstadt
Franziska-Braun-Straße 7, 64287 Darmstadt
Germany
nguyen-hoang@fsm.tu-darmstadt.de becker@fsm.tu-darmstadt.de

Abstract:
Bolted joints are widely used to connect safety relevant parts in the aeronautical industry and require precise stress analysis tools. If the joint has a fully symmetric setup with respect to the midplane a plane problem modelling is applicable. Focus of this paper is the analytical stress field determination and load transfer modelling of a finite dimensions bolted joint with isotropic material using the Airy stress function enabling cost-efficient computation. The load is introduced by sinusoidal radial stresses at the hole boundary idealising the bolt contact. It is led through the net section plane, in which crack initiation and propagation have to be avoided. This requires accurately calculated net section stresses carrying the whole load. To reach this aim the stress boundary conditions in load direction at the straight free edges must be fulfilled. To solve this first boundary value problem the stress field describing the load introduction is determined while neglecting the stress free boundary conditions at the straight edges. Then auxiliary functions are superimposed cancelling non-zero tractions in load direction at the straight edges and thus providing a physical force flux. Since traction boundary conditions perpendicular to the load direction are not covered inaccuracies in the stress solution may arise. Their criticality will be assessed by conducting a failure analysis in which predictions derived using the stresses of the present calculus are compared to literature values.

Keywords: Bolted joint, Composite laminates, Stress analysis, Failure Analysis, Airy stress function, Finite dimensions

1 Introduction

Bolted joints are a common joining technique in the aeronautical industry for reasons of inexpensive manufacturing and the possibility to disassemble. Drilling a hole introduces a stress-raiser requiring precise stress and failure assessment tools to ensure both structural integrity and a lightweight optimal design. The first step in structural assessment is determining the stresses followed by a failure analysis. The stress state is generally three-dimensional and capturing all failure mechanism factors is complex especially if intending an analytical modelling beneficial in terms of computational effort.

To reduce the complexity a two-dimensional in-plane idealisation is pursued incorporating the main relevant effects of the failure mechanism. This is applicable if the bolted joint connection contains a material behaviour without bending extension coupling and an overall symmetrical setup with respect to the midplane. The stress analysis of a pin-loaded hole has been analytically treated by many scientists with different level of complexity such as contact modelling with or without friction, material anisotropy or finite dimensions. An extensive stress analysis review can be found in [1] and [2] whereas [3] is more general and focusses on mechanical modelling including stress and failure analysis as well as experimental validation. The available stress solutions in many cases idealise the bolt contact by a sinusoidal radial stress distribution along the hole boundary. If the material is isotropic the plane elasticity problem can be approached using the Airy stress function, which has been performed by [4] for infinite dimensions providing a good approximation of the circumferential stresses at the hole boundary. Unfortunately the net section stresses in load direction relevant for local crack initiation prediction unphysically and rapidly converge to a value in compression. In [5] the stress field of both the infinite and the finite width joint is determined. The zero shear stress boundary condition at the hole is slightly violated. Furthermore the load transfer of a finite dimensions joint can not be adequately modelled only considering a finite width.

For problems involving an anisotropic material solutions have been developed using the Lekhnitskii complex potential formalism [6]. The infinite geometry pin-loaded hole without bending extension coupling is treated in [7] and further extended for any arbitrary load direction in [8]. A solution for the finite dimensions problem is developed in [9] using finite width correction factors. Drawback of this method are the violated stress boundary conditions at the free edges. A similar approach

doi: 10.25967/490004

has been implemented in [10] and [11]. The first shows good agreement in the circumferential stresses at the hole boundary in comparison to the finite element (FE) solution for rather larger dimensions $e/d = 9$ and $w/d > 4$ (ref. Fig. 1) whereas the latter only discusses stress concentration factors at the hole boundary. These may serve for local failure criteria but are not sufficient if intending to use criteria enabling to model the hole size effect. In [12] a finite dimensions connection is treated by approximating the rectangular plate geometry as an ellipse yielding good correlation to FE results in the circumferential stresses for $[\pm 45°]_s$ and $w/d = 3$ as well as for $[0°/90°]_s$ and $w/d = 5$. Bending extension coupling is modelled in [13] revealing good agreement to FE solution for $w/d = \{15, 45\}$ and $e/d = \{7.5, 37.5\}$ in which finite width effects are small or even have decayed. The method is extended to multilayered composites bolted joints with interference-fit under thermal load [14]. All the solutions summed up reveal agreement for rather larger dimensions if validated at all. To the authors' knowledge for $w/d \leq 4$ there exists no analytical approach to accurately determine the stress field especially the net section stresses essential for tension failure prevention, which is then not only validated using FE but also further established in a subsequent failure analysis.

These gaps shall be treated in the following for the stress field of a quasi-isotropic composite bolted joint with finite dimensions is derived using the Airy stress function. The stress solution is then used in a net section failure analysis likely to occur for small widths $w/d \leq 4$ [15]. In a first step the stress function describing the load introduction is determined for the infinite geometry neglecting stress free boundary conditions at the straight edges. For a full load transfer through the net section area at least the stress free boundary conditions in load direction need to be fulfilled. This is achieved by superimposing virtual auxiliary functions created by mirroring the load introduction field enabling full cancellation of non-zero stresses in load direction at the straight edges while maintaining the stress boundary conditions at the hole edge. Those boundary conditions perpendicular to the load direction at the straight edges do not play a role in the equilibrium in load direction and are thus not covered by the present method. To the authors' knowledge this approach is firstly used in the Theory of Elasticity and provides a convenient mean to deal with finite domain problems involving straight free edges. The resulting net section stresses will transfer the whole external load but nevertheless might be differently shaped in comparison to the FE solution fulfilling all stress boundary conditions. The criticality of those potential stress deviations is assessed by conducting a failure analysis using the Theory of Critical Distances (TCD, [16, 17]). Its performance is compared to experimental data as well as to predictions based on means of the finite fracture mechanics (FFM, [18]), which is applied for bolted joints in [19].

2 Determination of the stress field

The stress field for an isotropic pinned hole with finite dimensions as shown in Fig. 1 is developed. In doing so the quantity P_y denotes an external force per plate thickness applied in the vertical direction, w is the width, e the hole to end distance and d the hole diameter of the plate as well as of the bolt assuming no oversize or clearance. This problem setting is idealised as a first boundary value problem, whose stresses are determined using the Airy stress function.

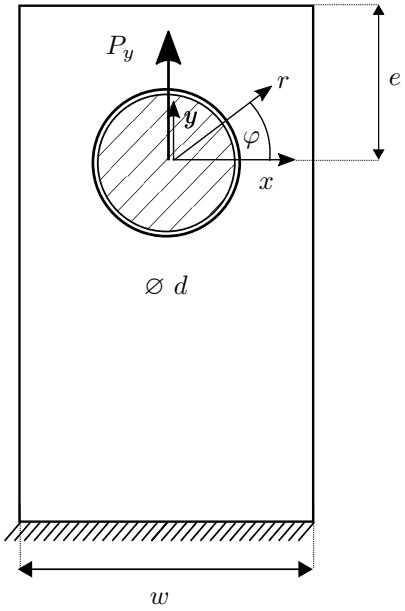

Fig. 1. Geometry of bolted joint.

2.1 Fundamentals of the Airy stress function

We assume a two-dimensional plane stress or plane strain problem with linear elastic and isotropic material behaviour. The governing equations of equilibrium, compatibility and Hooke's law can be then reduced to a single differential equation containing the Airy stress function F. For a plane stress problem with non existent body forces the function F needs to satisfy the following biharmonic equation [20, 21]:

(1)
$$\Delta\Delta F = 0 \qquad \text{with}$$

$$\Delta = \begin{cases} \dfrac{\partial^2 F}{\partial x^2} + \dfrac{\partial^2 F}{\partial y^2} & \text{in cartesian coordinates,} \\ \dfrac{\partial^2}{\partial r^2} + \dfrac{1}{r}\dfrac{\partial}{\partial r} + \dfrac{1}{r^2}\dfrac{\partial^2}{\partial \varphi^2} & \text{in polar coordinates.} \end{cases}$$

Functions F obeying the biharmonic equation are called biharmonic functions and were addressed in [22]. The plane stress components are calculated using

$$\sigma_x = \frac{\partial^2 F}{\partial y^2}, \qquad \sigma_y = \frac{\partial^2 F}{\partial x^2}, \qquad \tau_{xy} = -\frac{\partial^2 F}{\partial x \partial y}, \tag{2}$$

$$\sigma_r = \frac{1}{r}\frac{\partial F}{\partial r} + \frac{1}{r^2}\frac{\partial^2 F}{\partial \varphi^2}, \quad \sigma_\varphi = \frac{\partial^2 F}{\partial r^2}, \quad \tau_{r\varphi} = -\frac{\partial}{\partial r}\left(\frac{1}{r}\frac{\partial F}{\partial \varphi}\right). \tag{3}$$

Stress functions F are now to be chosen such that the corresponding stresses fulfil the given stress boundary conditions of a first boundary value problem.

2.2 Overview of the calculus

At first a bolt contact idealisation is presented providing the hole boundary stress conditions to satisfy. A stress function F_{LI} fulfilling them is then derived and represents the load introduction, whose force flux is spread in all directions reaching stress free conditions at infinity and therefore describes the pinned hole with infinite geometry. In the finite dimensions case, however, the force flux is directed through the net section area towards the clamp shown along the lower edge in Fig. 1. This load transfer is modelled by superimposing F_{LI} with auxiliary functions cancelling the tractions in load direction at the straight edges while keeping the hole boundary conditions unchanged.

2.3 Bolt contact idealisation

The bolt plate contact problem is idealised by a sinusoidal function in the radial direction and with the assumption of no friction and thus vanishing shear stresses at the hole boundary [23]. The complete boundary conditions read

$$\sigma_r(R,\varphi) = \begin{cases} -\frac{2}{\pi}\frac{F_y}{R}\sin(\varphi) & \text{for} \quad 0 \le \varphi \le \pi, \\ 0 & \text{for} \quad \pi \le \varphi \le 2\pi, \end{cases} \tag{4}$$

$$\tau_{r\varphi}(R,\varphi) = \quad 0 \qquad\qquad \text{for} \quad 0 \le \varphi \le 2\pi,$$

where $R = d/2$ denotes the hole radius. The hole boundary conditions shall be satisfied by F_{LI} representing the load introduction but also by the final finite bolted joint solution F.

2.4 Stress function F_{LI} modelling the load introduction

The field F_{LI} obeying the stress hole boundary conditions in Eq. (4) is developed. The free straight edges are not considered at this stage. As in [5] let us build two partial functions with

$$F_{\mathrm{LI}} = F_1 + F_2. \tag{5}$$

The first partial function represents a full sine in the radial stresses over the complete hole boundary while the latter yields a cosine Fourier series expansion of $|\sigma_{r1}(R,\varphi)|$ belonging to F_1. Since only cosine terms are used in the Fourier series both radial stresses $\sigma_{r1}(R,\varphi)$ and $\sigma_{r2}(R,\varphi)$ have the same behaviour along the upper circular boundary whereas at the lower they have a reversed sign and therefore superimposed lead to cancellation. This approach is illustrated in Fig. 2. Contrary to [5] both partial functions fulfil vanishing shear stresses at $r = R$.

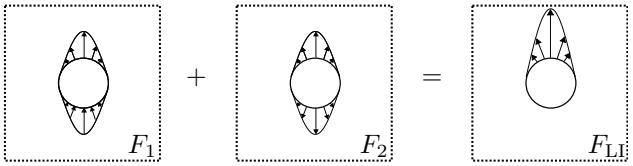

Fig. 2. Radial stresses at the hole boundary.

According to [4] the stress function F_1 reads

$$F_1 = a_{15}\, r\varphi\cos\varphi + b_{12}\, r \ln\frac{r}{R}\sin\varphi + b_{13}\frac{1}{r}\sin\varphi. \tag{6}$$

The corresponding stress components can be calculated using Eq. (2) and (3). The coefficients are determined by

$$\frac{b_{12}}{a_{15}} = \frac{1}{2}(1-\nu), \tag{7}$$

ensuring single-valued circumferential displacements u_φ [4, 20], with ν being the Poisson's ratio of the plate material,

$$\sigma_{r1}(R,\pi/2) = -\frac{1}{\pi}\frac{F_y}{R} \tag{8}$$

transferring half of the outer load and eventually

$$\tau_{r\varphi 1}(R,\varphi) = 0, \tag{9}$$

leading to vanishing shear stresses at the hole boundary. Normalising with respect to the reference stress $\sigma_0 = \frac{F_y}{d}$, F_1 is then expressed by

$$F_1 = \frac{R}{\pi}\left[r\varphi\cos\varphi + \frac{1}{2}(1-\nu)\, r \ln\frac{r}{R}\sin\varphi + \right. \\ \left. + \frac{1}{4}(1-\nu)\, R^2\frac{1}{r}\sin\varphi\right]\sigma_0. \tag{10}$$

The amount of the radial stresses $\sigma_{r1}(R,\varphi)$ shall now be expanded by a Fourier cosine series. Its corresponding stress function has the general form

$$F_2 = R^2\Bigg[b_2 \ln\frac{r}{R} + \sum_{n=1}^{N}\left\{A_{2,n}\left(\frac{R}{r}\right)^{2n} + B_{2,n}\left(\frac{R}{r}\right)^{2n-2}\right\}\cos 2n\varphi\Bigg]\sigma_0. \tag{11}$$

Let us represent $|\sigma_{r1}(R,\varphi)|$ by the Fourier series

$$\sigma_{r2}(R,\varphi)/\sigma_0 = \frac{f_{2,0}}{2} + \sum_{n=1}^{N^*} f_{2,n}\cos n\varphi, \tag{12}$$

$$\text{with}\quad f_{2,n} = \frac{1}{\pi}\frac{1}{\sigma_0}\int_0^{2\pi}\sigma_{r1}(R,\varphi)\cos n\varphi\,\mathrm{d}\varphi$$

$$= \begin{cases} 0 & \text{for odd } n, \\ -\dfrac{4}{\pi^2}\dfrac{1+\cos n\pi}{1-n^2} & \text{for even } n. \end{cases} \tag{13}$$

The Airy coefficients $A_{2,n}, B_{2,n}$ are obtained by deriving the radial stresses of F_2 and equating them with the Fourier series in Eq. (12) while taking into account that uneven $f_{2,n}$ are zero which yields

$$b_2 = \frac{f_{2,0}}{2}, \tag{14}$$

$$-2[n(2n+1)A_{2,n} + (n+1)(2n-1)B_{2,n}] = f_{2,2n}. \tag{15}$$

Furthermore ensuring $\tau_{r\varphi 2}(R,\varphi) = 0$ leads to

$$(2n+1)A_{2,n} + (2n-1)B_{2,n} = 0. \tag{16}$$

Using Eq. (15) and (16) the Airy stress coefficients are calculated by

$$A_{2,n} = -\frac{2n-1}{2n+1}B_{2,n},$$

$$B_{2,n} = \frac{1}{2}\frac{f_{2,2n}}{n(2n-1)-(n+1)(2n-1)}. \tag{17}$$

The stress field F_{LI} is now fully determined. In order to cancel the traction in load direction at the straight edges and thus leading the load transfer through the net section area towards the clamp auxiliary functions are developed and superimposed.

2.5 Finite geometry modelling using auxiliary stress functions

Let us investigate the free body diagram shown in Fig. 3 giving an idea about the stresses in the final solution.

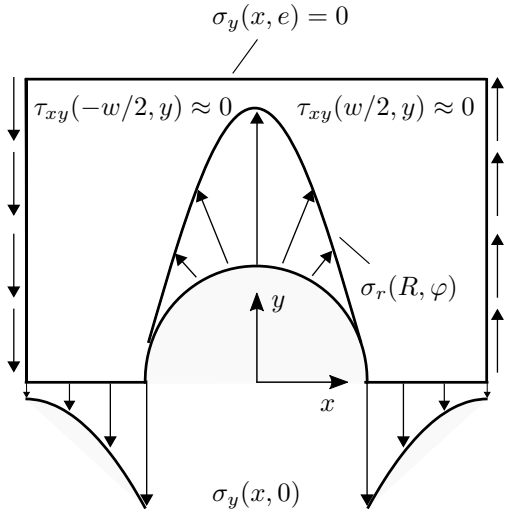

Fig. 3. Free form body. Only stresses relevant for equilibrium in load direction are shown.

For the transfer of the whole external load through the net section area its normal stresses $\sigma_y(x,0)$ must equilibrate F_y alone, which requires vanishing stresses in load direction at the straight edges. This is reached by introducing virtual neighbouring auxiliary plates created by mirroring the load introduction field $F_{\mathrm{LI}} = F_{\mathrm{LI}}^{11}$ and arranged as shown in Fig. 4.

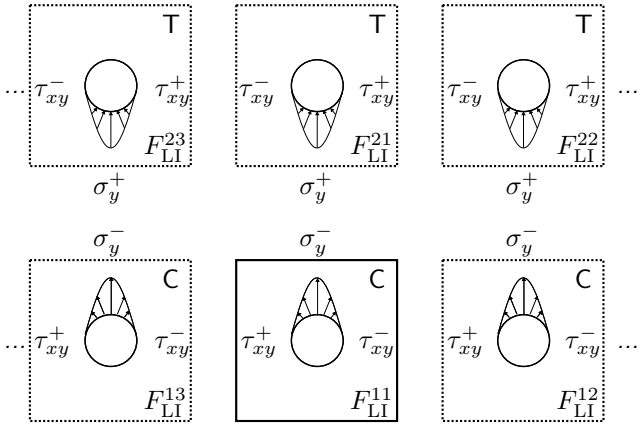

Fig. 4. Schematic how to arrange virtual auxiliary plates of $F_{\mathrm{LI}} = F_{\mathrm{LI}}^{11}$. C ≙ Compression, T ≙ Tension.

For cancellation of the normal stresses $\sigma_y^-(x,e)$ at the horizontal edge F_{LI}^{11} needs to be vertically copied, its loading reversed to tension and shifted by π along the hole boundary creating the auxiliary plate F_{LI}^{21}. For vanishing shear stresses $\tau_{xy}^{\mp}(\pm w/2,y)$ at the two vertical edges F_{LI}^{11} is horizontally mirrored creating F_{LI}^{12} and F_{LI}^{13}. Since the left auxiliary plate does not only cancel the shear stresses at $x=-w/2$ but also influences those at the opposite edge $x=w/2$ and vice versa for the right auxiliary plate and its opposite edge at $x=-w/2$ there will be a remaining rest at both vertical edges. Its magnitude will depend on the number of horizontally aligned auxiliary plates in use. If a periodic row of auxiliary plates

is superimposed the shear stresses will vanish. As the horizontal auxiliary plates will introduce further normal stresses σ_y^- at $y = e$ they need to be vertically copied like F_{LI}^{11} ensuring full cancellation. The auxiliary plates for the partial fields F_1 and F_2 of the load introduction field F_{LI} can be calculated by

(18)
$$F_k^{ij}(x,y) = \underbrace{(-1)^{i+1}}_{\substack{\text{Tension/}\\ \text{Compression}}} \cdot F_k\Big(\underbrace{(-1)^{i+1}x_j, (-1)^{i+1}y_i}_{\text{load shifting along hole}}\Big),$$

with

$$\begin{aligned}[x_j] &= [x_1 \quad x_2 \quad x_3 \quad x_4 \quad ...] \\ &= [x \quad x-w \quad x+w \quad x-2w \quad ...]\,, \end{aligned} \tag{19}$$

$$[y_i] = [y_1 \quad y_2] = [y \quad y-2e]\,. \tag{20}$$

The superimposed field of the load introduction then is obtained using

$$F_{\mathrm{LI}}^{\mathrm{sup}} = \sum_{k=1}^{n_k=2} \underbrace{\sum_{i=1}^{n_y=2} \sum_{j=1}^{n_x} F_k^{ij}}_{=F_k^{\mathrm{sup}}}, \tag{21}$$

with F_k^{sup} being a superimposed partial field. The quantity n_x denotes the total number of horizontally, n_y the total number of vertically aligned plates. For the specific bolted joint problem n_x is considered as sufficiently large if there is less than $1\ \%$ loss in the load transfer due to remaining shear stresses at the vertical straight edges in the superimposed load introduction field $F_{\mathrm{LI}}^{\mathrm{sup}}$. This is expressed by

$$\frac{2}{F_y}\left| \int_0^e \sum_{i}^{n_y=2} \sum_{j}^{n_{x,\min}} \Big(\tau_{xy1}^{ij}(\pm w/2, y) + \tau_{xy2}^{ij}(\pm w/2, y)\Big)\,\mathrm{d}y \right| \leq 0.01, \tag{22}$$

and the smallest n_x fulfilling Eq. (22) leads to $n_{x,\min}$.

2.6 Correction functions to mitigate deviations in the hole boundary conditions

Beyond the desired effect of stress cancellation at the free edges the auxiliary plates also affect the hole boundary conditions fulfilled by the unmirrored load introduction field F_{LI}. The arising deviations in the hole boundary stresses are mitigated by superimposing a correction field F_3 expanding the deviations in a Fourier series. Since this new field disturbs zero stress boundary conditions in load direction at the free straight edges it needs to be mirrored in the same way as F_{LI}, which again results in slightly violated hole boundary conditions. Iterating this procedure by introducing further correction functions $F_{k>3}$ and mirroring them leads to vanishing deviations in the hole boundary conditions. The full solution F that correctly models the load introduction as well as fulfils the boundary conditions in load direction at the free edges with the smallest computational effort is eventually assembled by

$$F = \sum_{i}^{n_y=2} \sum_{j}^{n_{x,\min}} \sum_{k}^{n_{k,\min}} F_k^{ij}. \tag{23}$$

Table 1
Stress fields assembling the full solution.

stress field	task at hole boundary
F_1	represents full sine in radial stresses
F_2	Fourier series expansion of $\sigma_{r1}(R,\varphi)$
$F_{\mathrm{LI}} = F_1 + F_2$	sinusoidal bolt load introduction
$F_{k\geq 3}$	correction of deviating stresses in F_{k-1}^{sup}

The task of each partial field F_k is summarised in Tab. 1. The minimum number of required correction functions $n_{k,\min}$ is considered as sufficiently large if the relations

$$\begin{aligned} \chi_{\sigma_r} &= \frac{R}{F_y}\left|\int_0^{\pi} \sigma_r(R,\varphi)\sin\varphi\,\mathrm{d}\varphi\right| = 1, \\ \psi_{\sigma_r} &= \frac{R}{F_y}\int_{\pi}^{2\pi} \sqrt{\sigma_r(R,\varphi)^2}\sin\varphi\,\mathrm{d}\varphi \leq 0.01, \\ \psi_{\tau_{r\varphi}} &= \frac{R}{F_y}\int_0^{2\pi} \sqrt{\tau_{r\varphi}(R,\varphi)^2}\cos\varphi\,\mathrm{d}\varphi \leq 0.01, \end{aligned} \tag{24}$$

with the load transfer ratios involving those stresses of the full superimposed solution F are true. A load transfer value $\chi_{\sigma_r} = 1$ means that the external load is fully introduced by the radial sinusoidal stresses at the hole boundary. The ratios ψ_{σ_r} and $\psi_{\tau_{r\varphi}}$ are a means to assess undesirable non-zero oscillations at $r = R$. Inaccurate load transfer values of polar stresses indicate that the number of correction functions $n_{k,\min}$ shall be increased. A final check of the force flux through the net section plane is performed by quantifying the load transfer ratio

$$\chi_{\sigma_y} = \frac{2}{F_y}\int_R^{w/2} \sigma_y(x,0)\,\mathrm{d}x \quad \text{with} \quad 0.98 \leq \chi_{\sigma_y} \leq 1. \tag{25}$$

A too small χ_{σ_y} means that the shear stresses cancellation at the straight vertical edges is insufficient which can be cured by increasing the number of horizontal auxiliary plates $n_{x,\min}$. Note that after its increase the iterative correction function routine must be recalculated since the hole boundary stress deviations depend on the number of auxiliary plates. The flowchart in Fig. 5 summarises the overall finite bolted joint calculation method.

Let us continue with the determination of the correction functions $F_{k\geq 3}$. Their radial and shear stresses

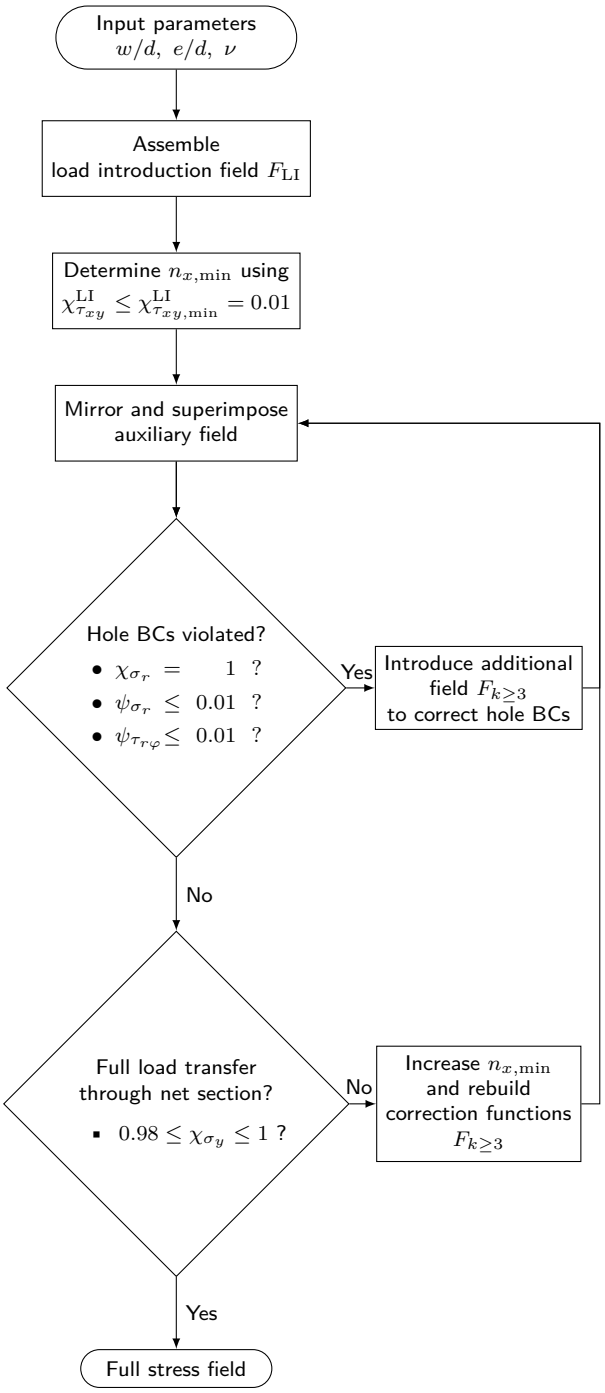

Fig. 5. Flowchart of the bolted joint calculation method.

Table 2
Deviating stresses at hole boundary to be expanded.

correction field	$\sigma^{\mathrm{dev}}_{rk}(R,\varphi)$	$\tau^{\mathrm{dev}}_{r\varphi k}(R,\varphi)$
F_3	$\sigma_{r1}+\sigma_{r2}-\sigma^{\mathrm{sup}}_{r1}-\sigma^{\mathrm{sup}}_{r2}$	$-\tau^{\mathrm{sup}}_{r\varphi 1}-\tau^{\mathrm{sup}}_{r\varphi 2}$
F_4	$\sigma_{r3}-\sigma^{\mathrm{sup}}_{r3}$	$\tau_{r\varphi 3}-\tau^{\mathrm{sup}}_{r\varphi 3}$

at the hole boundary expand the deviations caused by the previously superimposed auxiliary fields enabling their mitigation. Taking into account that the bolted joint problem is symmetric to the y-axis the expansions read

$$\sigma_{rk}(R,\varphi)/\sigma_0 = \frac{f^{\sigma_r}_{k,0}}{2} + \sum_{n=1}^{N} f^{\sigma_r}_{k,2n}\cos 2n\varphi + \sum_{n=0}^{N} g^{\sigma_r}_{k,2n+1}\sin(2n+1)\varphi, \tag{26}$$

$$\tau_{r\varphi k}(R,\varphi)/\sigma_0 = \sum_{n=0}^{N} f^{\tau_{r\varphi}}_{k,2n+1}\cos(2n+1)\varphi + \sum_{n=1}^{N} g^{\tau_{r\varphi}}_{k,2n}\sin 2n\varphi \tag{27}$$

with the coefficients

$$\begin{aligned} f^{\sigma_r}_{k,n} &= \frac{1}{\pi}\frac{1}{\sigma_0}\int_0^{2\pi} \sigma^{\mathrm{dev}}_{rk}(R,\varphi)\cos n\varphi\,\mathrm{d}\varphi, \\ g^{\sigma_r}_{k,n} &= \frac{1}{\pi}\frac{1}{\sigma_0}\int_0^{2\pi} \sigma^{\mathrm{dev}}_{rk}(R,\varphi)\sin n\varphi\,\mathrm{d}\varphi, \\ f^{\tau_{r\varphi}}_{k,n} &= \frac{1}{\pi}\frac{1}{\sigma_0}\int_0^{2\pi} \tau^{\mathrm{dev}}_{r\varphi k}(R,\varphi)\cos n\varphi\,\mathrm{d}\varphi, \\ g^{\tau_{r\varphi}}_{k,n} &= \frac{1}{\pi}\frac{1}{\sigma_0}\int_0^{2\pi} \tau^{\mathrm{dev}}_{r\varphi k}(R,\varphi)\sin n\varphi\,\mathrm{d}\varphi. \end{aligned} \tag{28}$$

For the geometrical configurations investigated and the given accuracy degree two iterations are sufficient to satisfy the stress boundary conditions at the hole and those in load direction at the straight edges. Tab. 2 lists the particular stress deviations to be expanded by the correction functions $F_{k\geq 3}$. The general form for an Airy stress field F_k describing the Fourier expansions in Eq. (26) and (27) is expressed by

$$\begin{aligned} F_k(r,\varphi) = R^2\Bigg[& b^{\sigma_r}_k \ln\frac{r}{R} + c^{\sigma_r}_k \frac{r}{R}\,\varphi\cos\varphi + \\ & + d^{\sigma_r}_k \frac{r}{R}\ln\frac{r}{R}\sin\varphi + d^{\tau_{r\varphi}}_k \frac{R}{r}\sin\varphi + \\ & + \sum_{n=1}^{N}\left\{ A_{k,n}\left(\frac{R}{r}\right)^{2n} + B_{k,n}\left(\frac{R}{r}\right)^{2n-2}\right\}\cos 2n\varphi + \\ & + \sum_{n=1}^{N}\left\{ C_{k,n}\left(\frac{R}{r}\right)^{2n+1} + \right. \\ & \left. + D_{k,n}\left(\frac{R}{r}\right)^{2n-1}\right\}\sin(2n+1)\,\varphi\Bigg]\,\sigma_0. \end{aligned} \tag{29}$$

Equating the coefficients in the Fourier series representation in Eq. (26) and (27) with those of $\sigma_{rk}(R,\varphi)$ and $\tau_{r\varphi k}(R,\varphi)$ belonging to F_k while taking into account single valued displacements [4, 20] expressed by

$$\frac{d^{\sigma_r}_k}{c^{\sigma_r}_k} = \frac{1}{2}(1-\nu), \tag{30}$$

yields

(31)

$$b_k^{\sigma_r} = \frac{1}{2} f_{k,0}^{\sigma_r}, \qquad c_k^{\sigma_r} = -\frac{1}{2}\left(f_{k,1}^{\tau_{r\varphi}} + g_{k,1}^{\sigma_r}\right),$$
$$d_k^{\sigma_r} = \frac{1}{2}(1-\nu)\, c_k^{\sigma_r}, \qquad d_k^{\tau_{r\varphi}} = \frac{1}{2}\left(f_{k,1}^{\tau_{r\varphi}} + d_k^{\sigma_r}\right),$$

(32)

$$A_{k,n} = -\frac{1}{n(2n+1)}\left[\frac{1}{2} g_{k,2n}^{\tau_{r\varphi}} + n(2n-1)\, B_{k,n}\right],$$

$$B_{k,n} = \frac{1}{2}\frac{g_{k,2n}^{\tau_{r\varphi}} - f_{k,2n}^{\sigma_r}}{2n-1},$$

$$C_{k,n} = \frac{1}{n+1}\left[\frac{f_{k,2n+1}^{\tau_{r\varphi}}}{2(2n+1)} - nD_{k,n}\right],$$

$$D_{k,n} = -\frac{1}{4n}\left(g_{k,2n+1}^{\sigma_r} + f_{k,2n+1}^{\tau_{r\varphi}}\right).$$

With that all functions for the full solution are determined. Results for different geometrical properties w/d and e/d are presented and verified using Finite Element analysis in the subsequent section.

3 Discussion of the stress results

In this section the results for the joint configurations with the geometrical dimensions in the range $w/d = \{3, 20\}$ and $e/d = \{3, 10\}$ are presented and verified using a Finite Element model implemented in ABAQUS. The mesh contains CPS8 continuum plane stress elements with 8 nodes. A sinusoidal load in the radial stresses modelling the contact idealisation is applied at $r = R$. Convergence in the stresses is reached for 72 elements at the hole boundary. Fig. 6 shows the FE model for $w/d = 3,\ e/d = 3$ and introduces the dimensionless coordinate

(33)
$$\xi = \frac{x - R}{w/2 - R},$$

with $\xi = 0$ at the hole boundary and $\xi = 1$ at the free edge.

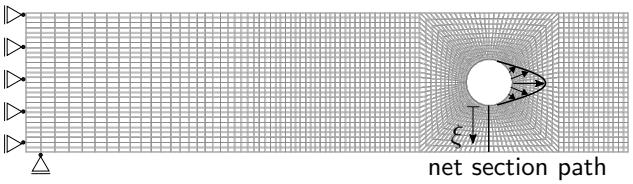

Fig. 6. Finite Element model for $w/d = 3,\ e/d = 3$.

To qualitatively investigate the effect of the auxiliary plates on the load transfer let us exemplarily plot the force flux of the stress vector

(34)
$$\vec{t_y} = \begin{bmatrix} \sigma_x & \tau_{xy} \\ \tau_{xy} & \sigma_y \end{bmatrix} \cdot \begin{bmatrix} 0 \\ -1 \end{bmatrix} = -\begin{bmatrix} \tau_{xy} \\ \sigma_y \end{bmatrix},$$

for $w/d = 20,\ e/d = 10$ shown in Fig. 7.

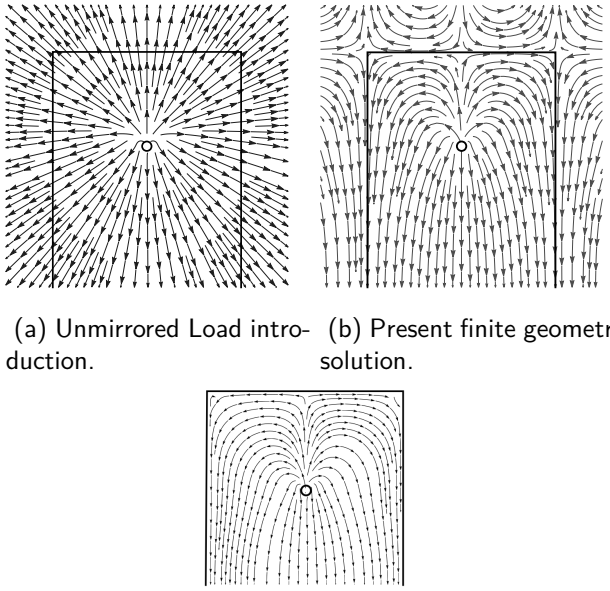

(a) Unmirrored Load introduction. (b) Present finite geometry solution.

(c) FE solution.

Fig. 7. Force flux of stress vectors $\vec{t_y}$ for bolted joint with $w/d = 20,\ e/d = 10,\ n_{x,\min} = 23$.

If superimposing the auxiliary fields the force flux becomes tangent to the straight boundaries as in the Finite element solution thus providing a physical load transfer. For further quantitative approval the load transfer ratios are analysed. For the different bolted joint setups the presented calculus leads to load transfer ratios within the range

(35)
$$\chi_{\sigma_r} = 1, \quad 0.98 \leq \chi_{\sigma_y} \leq 0.99, \quad \psi_{\sigma_r}, \psi_{\tau_{r\varphi}} < 0.005,$$

fulfilling the requirements defined in Eq. (24), (25) and therefore confirming the methodology. Fig. 8 illustrates $n_{x,\min}$ with respect to the geometric properties leading to these load transfer value ranges.

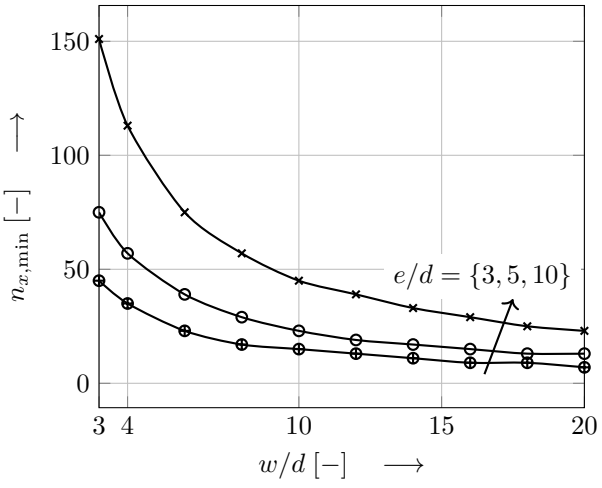

Fig. 8. Minimum number of horizontal plates $n_{x,\min}$.

The minimum number of horizontal plates $n_{x,\min}$ increases with a smaller value w/d since the shear stress boundary conditions are more violated than in wider joints requiring additional horizontal auxiliary plates for cancellation of $\tau_{xy}(\pm w/2, y)$. Furthermore $n_{x,\min}$ increases with e/d. A small relative hole distance e/d requires the auxiliary plates F_{2j} being located near the original vertical joint boundaries at $x = \pm w/2 \wedge y \leq e$. The shear stresses $\tau_{xy}^{2j}(\pm w/2, y)$ of F^{2j} have a reversed sign in comparison to the field F^{1j} and do not decay as rapidly as in joint models with larger e/d. Therefore they contribute more significantly to the shear stress cancellation of the horizontally aligned auxiliary plates F^{1j}. Hence fewer horizontal plates are required to obtain a given shear stress cancellation ratio $\chi_{\tau_{xy}}$. Refer to Fig. 4 for further illustration. Let us investigate the circumferential stresses and the net section stresses relevant for the crack initiation assessment shown in Fig. 10.

Generally speaking the wider the dimension properties the better the agreement in both stress components is observed. Peaks in the hoop stresses at $\varphi = \{0,\, \pi/2,\, \pi,\, 3/2\,\pi\}$ as well as the net section stresses $\sigma_y(x, 0)$ deviate the more the smaller the dimensions are chosen. Deviations are due to non-zero stress boundary conditions normal to the load direction at the straight edges not covered by the present calculus, in particular $\tau_{xy}(x, e) \neq 0$ and $\sigma_x(\pm w/2, y) \neq 0$. This is further confirmed by applying these non-zero tractions additionally to the sinusoidal loading in the FE model, which is done for all configurations except for $w/d = 20$, $e/d = 10$ yielding only very slight stress deviations. The corresponding stress solution then coincides with that of the present calculus apart from small differences (ref. to Fig. 10). They arise since a load transfer value $\chi_{\sigma_y} \geq 0.98$ has been considered as sufficient. To assess how critical the stress deviations are a net section failure analysis using the present solution as well as the numerical reference is performed.

4 Failure analysis: comparison to the experiment

Let us conduct a failure analysis by means of the Theory of Critical Distances (TCD) being capable to capture the hole size effect in contrast to local criteria comparing the maximum stress with the strength. Using the line method the average net section stresses

$$\overline{\sigma}_y(\tilde{r_c}) = \frac{1}{\tilde{r_c}} \int_0^{\tilde{r_c}} \sigma_y(x^*, 0)\, \mathrm{d}x^* \quad \text{with } x^* = x - R \tag{36}$$

are considered. Herein $\tilde{r_c}$ represents an arbitrary hole distance. Failure is then postulated if the average net section stress within the critical hole distance $\tilde{r_c} = r_c$ is equal to the longitudinal tensile strength X_T^L of the plain material,

$$\overline{\sigma}_y(r_c) = X_T^L. \tag{37}$$

At first the characteristic distance needs to be determined. Then a failure analysis is conducted and the predicted failure stresses are compared to experimental data.

4.1 Determination of the characteristic distance

The characteristic distance r_c is calibrated using the stress field and the experimentally determined failure load for a specific bolted joint configuration [16]. It is therefore a non-physical quantity and generally not applicable to other joint configurations but possibly to a certain extent. For our study the experiment NT2 performed in [19] is chosen to calibrate r_c. This test setting involves the composite plate material Hexcel IM7-8552 with the layup $[90°/0°/\pm 45°]_{3s}$ providing quasi-isotropic material behaviour. Its nominal thickness is $t = 3$ mm. Further test specifications can be taken from Tab. 3.

Table 3
Test data from [19].

Test ID	d [mm]	w/d [-]	e/d [-]	σ_{F} [MPa]
NT2	6	1.75	5.83	466.2
NT3	6	2	4.17	526.7

The quantity σ_{F} denotes the failure stress with $\sigma_{\mathrm{F}} = P_{y,\mathrm{F}}/d$ where $P_{y,\mathrm{F}}$ represents the external load at failure. The corresponding stress field at failure is derived using both FE software and the present calculus. The characteristic distances $r_{c,\mathrm{Airy}}$ and $r_{c,\mathrm{FE}}$ are those distances where the corresponding average stresses $\overline{\sigma}_y(\tilde{r_c})$ reach $X_T^L = 845.1$ MPa. Refer to Fig. 9 for further illustration. Large deviations arise since the ratio $w/d = 1.75$ is very small and non-zero tractions perpendicular to the load direction uncovered by the calculus strongly affect the net section stresses.

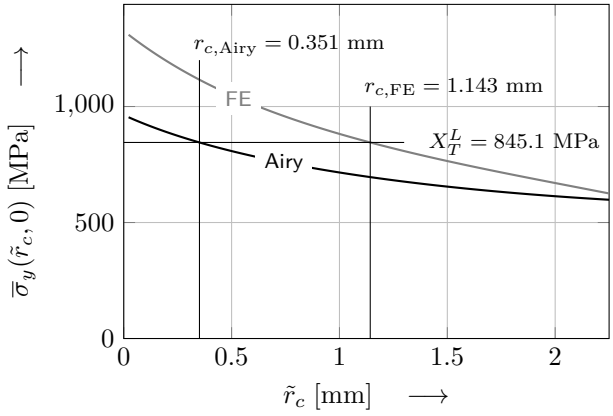

Fig. 9. Calibration of characterisitc distances using averaged net section stresses at failure of experiment NT2.

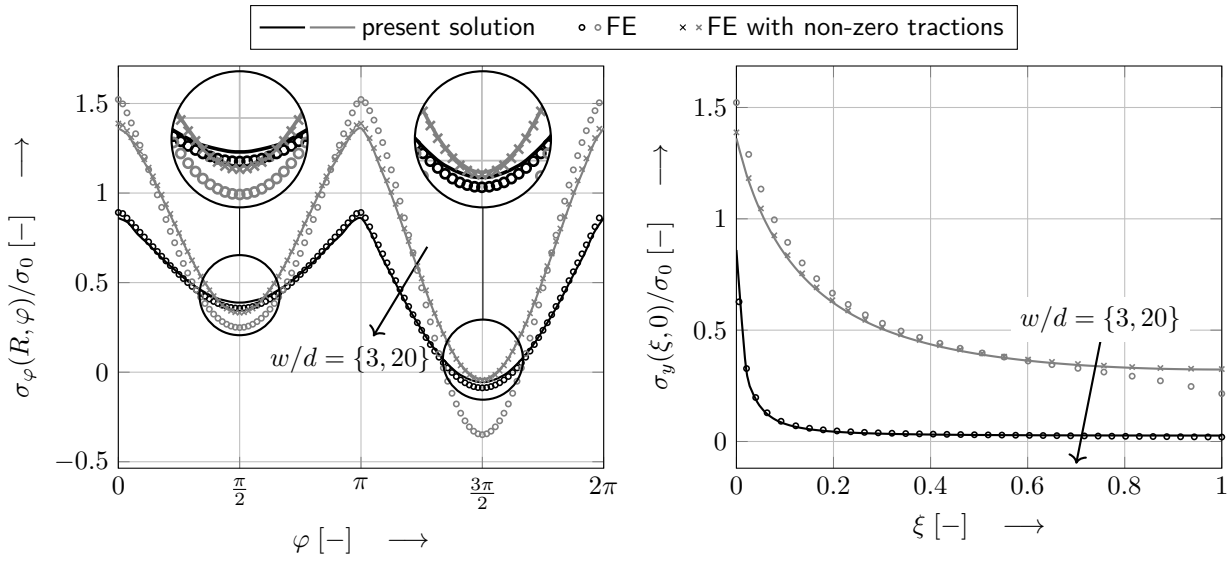

(a) $e/d = 10$

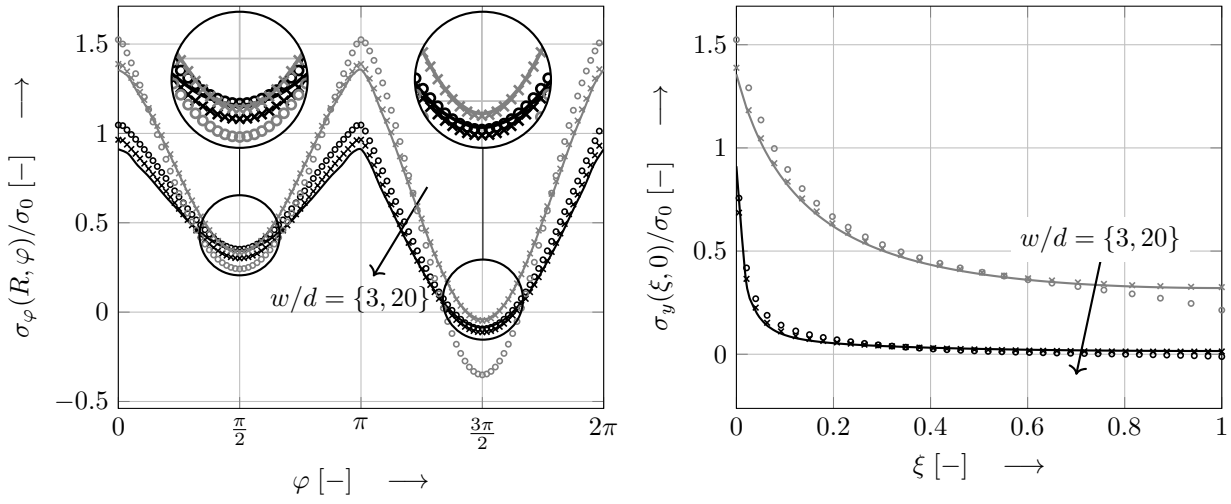

(b) $e/d = 3$

Fig. 10 Circumferential and net section stresses.

4.2 Comparison to experimental data

A failure analysis is conducted using the previously calculated characteristic distances. The failure stress for the test setting NT3 is predicted based on both analytically and numerically obtained stresses. It is found by scaling the external load such that the corresponding average net section stresses reach X_T^L at the characteristic distances. The normalised net section stresses are shown in Fig. 11. The dimensionless characteristic distances are calculated by

$$\xi_{r_c} = \frac{r_c}{w/2 - R}. \tag{38}$$

Tab. 4 compares the predicted bearing stresses at failure using their deviations normalised to the experimental value.

Table 4
Failure stresses for NT3.

	Airy	FE	FFM	Exp
σ_F [MPa]	540.6	569.1	549.5	526.7
ϵ [-]	2.6 %	8.1 %	4.3 %	-

A good agreement is observed if using the TCD with calibrated characteristic distance involving stresses based on the present solution (TCD-Airy). Since the corresponding failure stress prediction yields a deviation even smaller than those based on numerically calculated stresses (TCD-FE) the calibration approach can be considered as capable to cope with erroneous net section stresses of the present solution for the particular joint configuration. Further tests with different values for d and w/d should be performed to assess the present

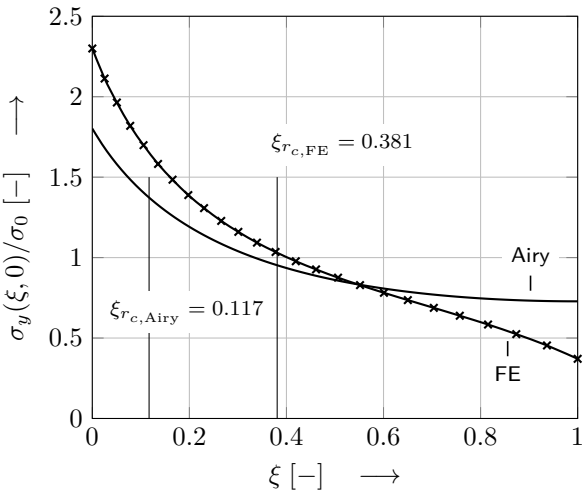

Fig. 11. Normalised net section stresses for NT3.

method's capabilities. Results derived by means of the Finite Fracture Mechanics (FFM) performed in [19] are also shown. Note that the TCD-Airy coincidentally leads to a prediction better than the FFM although the latter unifies both stress and energy criterion contrary to the TCD and is therefore the more sophisticated crack propagation model. Let us now investigate the predictions for different diameters and analyse how well the hole size effect is modelled by the TCD approach.

5 Failure analysis: modelling of the hole size effect

The failure stress is predicted for joint configurations with the same ratios $w/d,\ e/d$ as in NT3 but with different bolt diameter d. The predictions are based on stresses derived using the present calculus as well as FE software. The methodology to determine the failure load is analogous to previous section. The relative characteristic distance ξ_{r_c} where the stress failure criterion is evaluated decreases the larger d and vice versa. Since there are no experimental failure loads with respect to different diameters accessible to the authors those failure stresses calculated by means of the FFM published in [19] are reproduced and used as reference.

In the context of FFM [18] the initiation of a crack of the finite length Δa is assumed which instantaneously and unstably propagates if both stress and energy criteria are fulfilled. This condition is called coupled or hybrid criterion established in [24] and generally yields an optimisation problem to determine the minimal load and the corresponding crack length leading to unstable crack initiation. The bolted joint problem contains a monotonic decrease of the stresses and a monotonic increase of the energy release rate with respect to Δa. Using the dimensionless length $\Delta\xi = \Delta a/(w/2 - R)$ the coupled criterion simplifies then to the conditions

$$\begin{aligned} &\frac{1}{\Delta\xi}\int_0^{\Delta\xi} \sigma_y(\xi,0)\,\mathrm{d}\xi = X_L^T \\ &\wedge \quad \int_0^{\Delta\xi} K_{\mathrm{I}}^2(\xi)\,\mathrm{d}\xi = \int_0^{\Delta\xi} K_{\mathrm{IC}}^2(\xi)\,\mathrm{d}\xi \end{aligned} \tag{39}$$

where K_{I} denotes the mode I stress intensity factor of a newly initiated crack. $K_{\mathrm{IC}}(\xi)$ represents the R-curve for which a Gompertz function is used modelling a crack length dependency of the fracture toughness. This is important if the crack length is of the same order as the process zone l_{pz} which particularly occurs for small hole diameters [19].

Fig. 12 shows a comparison between FFM and TCD failure stresses with respect to the hole diameter d. The bearing cut-off is set at $\sigma_{\mathrm{F}} = 700$ MPa similar to [19]. Beyond this limit bearing failure occurs and corresponding criteria instead those of the net section crack initiation must be used. Furthermore the deviations normalised to the FFM are plotted in Fig. 13. A deviation limit of $|\epsilon| \leq 10\ \%$ is considered as tolerable giving us the diameter range in which the failure criteria can be used. This is further illustrated in Fig. 14.

The TCD-FE prediction is almost coinciding with the FFM reference starting with $d \geq 17$ mm for $w/d = 2$ and concerning $w/d = 3$ in the whole failure stress range below the bearing cut-off. Predictions using the TCD-Airy fulfil the deviation limit for rather small diameter $1\ \mathrm{mm} \leq d \leq 15\ \mathrm{mm}$ in the case $w/d = 2$ and can be used within a range where the TCD-FE approach fails. Beyond this diameter range the TCD-Airy lacks in accuracy. Contrary for $w/d = 3$ the TCD-Airy can be used for $8\ \mathrm{mm} \leq d \leq 354\ \mathrm{mm}$. The TCD-FE involves deviations converging with increasing d to a value smaller than the limit and are also applicable for $d > 50$ mm beyond the range investigated.

Let us further analyse the methodology of the various approaches to understand why they yield different predictions. The TCD is purely based on a stress criterion which is evaluated at a certain characteristic hole distance invariant to the hole diameter. Contrary as shown in Fig. 15 for various w/d configurations the FFM additionally incorporating the energy criterion reveals the crack length Δa and therefore the location where the stress criterion is evaluated being dependant of the hole diameter d. Beyond a certain hole diameter the curves $\Delta a(d)$ take a shape which can be approximated by a constant plateau value. The TCD-FE yields for this range accurate predictions since the corresponding characteristic distance $r_{c,\mathrm{FE}} = 1.143$ mm lies near the plateau confirming the calibration methodology.

In the frame of the TCD-Airy the prediction accuracy is affected by the erroneous net section stresses as well as by the characteristic distance $r_{c,\mathrm{Airy}} = 0.351$ mm of

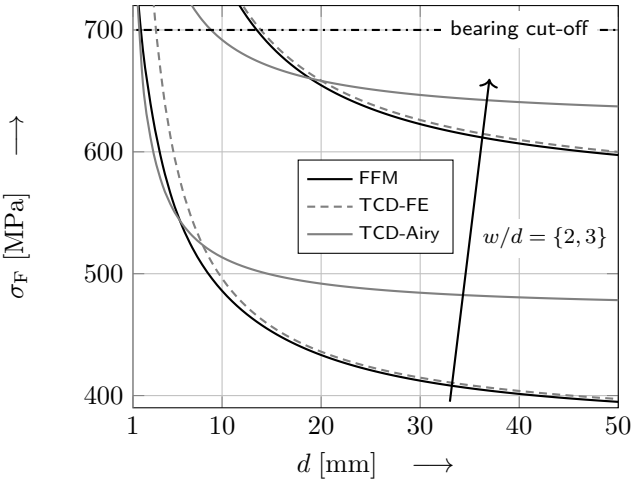

Fig. 12. Predicted stresses at failure.

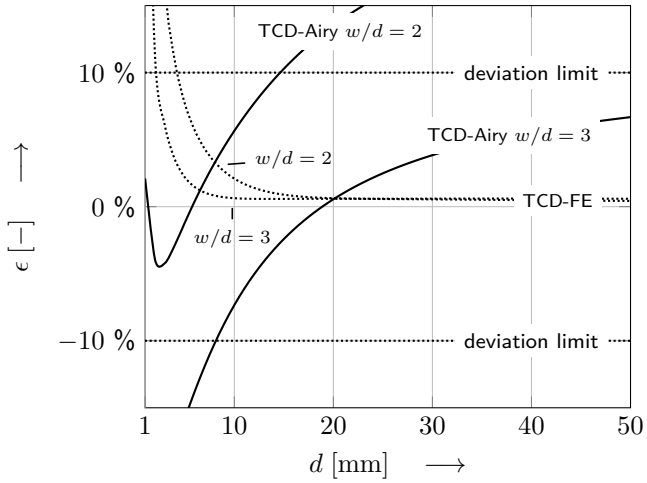

Fig. 13. Deviations of predicted failure stresses to FFM.

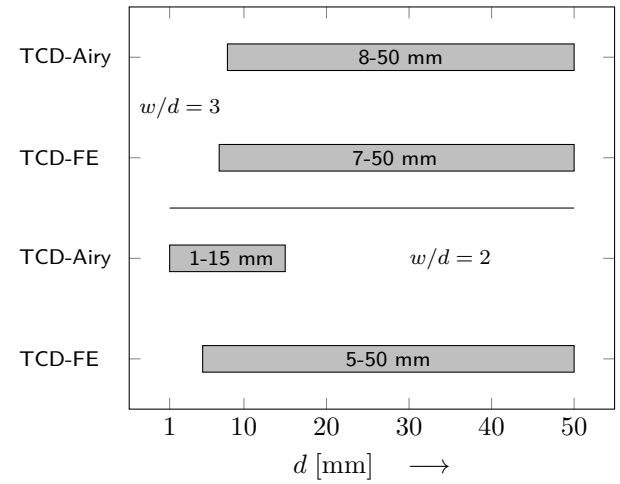

Fig. 14. Diameter range yielding $|\epsilon| \leq 10\ \%$.

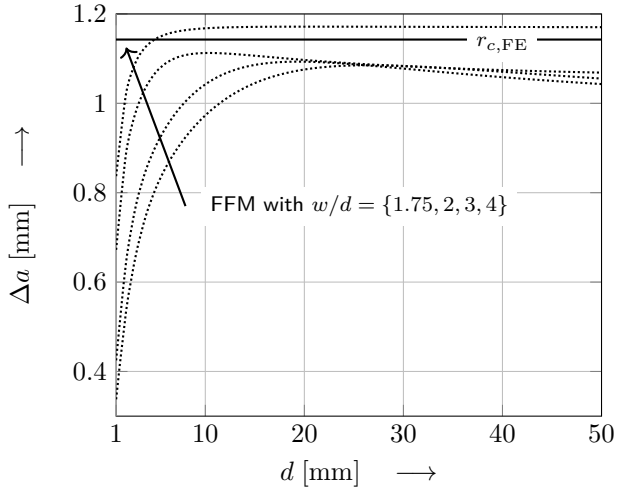

Fig. 15. Crack length Δa using FFM approach in [19].

the TCD-Airy lying outside the value range of Δa. Depending on the way how these impacts interact the final prediction might be either worse, unchanged or even better than the TCD-FE. Concerning $w/d = 2$ the TCD-Airy is even applicable within $1\ \mathrm{mm} \leq d \leq 15\ \mathrm{mm}$ partially lying outside the plateau where its numerical counterpart ascends the deviation limit. Regarding $w/d = 3$ the TCD-Airy yields an acceptable prediction for a diameter range similar to the TCD-FE but nevertheless with slightly higher deviations. For further validation of the hole size effect modelling using the present calculus experiments should be conducted since the FFM is just a model of crack propagation mechanisms occurring in real structures.

6 Conclusion

In the present paper the stress field for a finite bolted joint with quasi-isotropic composite material under in-plane loading is determined using the Airy stress function. The bolt contact is idealised by a sinusoidal radial stress distribution at the hole boundary. To obtain the solution use is made of auxiliary functions cancelling non-zero tractions in load direction at the free edges. Thus the force flux of the finite joint is modelled in a realistic manner. The stresses of the present solution are used in a subsequent net section failure analysis to further assess inaccuracies of the stresses. They arise since the stress boundary conditions perpendicular to the load direction are not covered. As failure criterion the Theory of Critical Distances is chosen using characteristic distances calibrated from the experimental failure load. The predictions yield deviations $|\epsilon| \leq 10\ \%$ for $w/d = 2$ in the diameter range $1\ \mathrm{mm} \leq d \leq 15\ \mathrm{mm}$ and concerning $w/d = 3$ within $8\ \mathrm{mm} \leq d \leq 354\ \mathrm{mm}$ in comparison to predictions in [19] derived by means of the finite fracture mechanics.

References

[1] F. Matthews, Theoretical stress analysis of mechanically fastened joints, Elsevier Applied Science Publishers Ltd, Joining Fibre-Reinforced Plastics, (1987) 65–103.

[2] P. Camanho, F. Matthews, Stress analysis and strength prediction of mechanically fastened joints in FRP: a review, Composites Part A: Applied Science and Manufacturing 28 (6) (1997) 529 – 547.

[3] P. Camanho, M. Lambert, A design methodology for mechanically fastened joints in laminated composite materials, Composites Science and Technology 66 (2006) 3004–3020.

[4] W. G. Bickley, The Distribution of Stress Round a Circular Hole in a Plate, Philosophical Transactions of the Royal Society of London 227 (1928) 383–415.

[5] R. Knight, The action of a rivet in a plate of finite breadth, Philosophy Magazine 19 (Series 7) (1935) 517–540.

[6] S. Lekhnitskii, Anisotropic plates, Gordon and Breach Science Publishers, 1968.

[7] T. De Jong, Spanningen rond een gat in een elastisch orthotrope of isotrope plaat, belast door een pen die zich daarin wrijvingsloos kan bewegen, Technische Hogeschool Delft, Afdeling der Luchtvaart-en Ruimtevaarttechniek, Rapport LR-223.

[8] T. De Jong, H. A. Vuil, Stresses around pin-loaded holes in elastically orthotropic plates with arbitrary load direction, Delft University of Technology, Department of Aerospace Engineering, Report LR-333.

[9] T. De Jong, Stresses around pin-loaded holes in elastically orthotropic or isotropic plates, Journal of Composite Materials 11 (1977) 313–331.

[10] J. Ogonowski, Effect of variances and manufacturing tolerances on the design strength and life of mechanically fastened composite joints AFWAL-TR-81-3041, 3, Technical report, McDonnell Aircraft Company (1981).

[11] C. Echavarria, P. Haller, A. Salenikovich, Analytical study of a pin–loaded hole in elastic orthotropic plates, Composite Structures 79 (1) (2007) 107 – 112.

[12] J. Kratochvil, W. Becker, Structural analysis of composite bolted joints using the complex potential method, Composite Structures 92 (10) (2010) 2512 – 2516.

[13] B. Grüber, W. Hufenbach, et al., Stress concentration analysis of fibre-reinforced multilayered composites with pin-loaded holes, Composites Science and Technology 67 (2007) 1439–1450.

[14] B. Grüber, M. Gude, et al., Calculation method for the determination of stress concentrations in fibre-reinforced multilayered composites due to metallic interference-fit bolt, Journal of Composite Materials 52 (18) (2018) 2415–2429.

[15] L. J. Hart-Smith, Mechanically-fastened joints for advanced composites — phenomenological considerations and simple analyses (1980) 543–574.

[16] J. M. Whitney, R. J. Nuismer, Stress fracture criteria for laminated composites containing stress concentrations, Journal of Composite Materials 8 (1974) 253–265.

[17] D. Taylor, The Theory of Critical Distances, Elsevier Science, 2007.

[18] P. Weißgraeber, D. Leguillon, W. Becker, A review of finite fracture mechanics: Crack initiation at singular and non-singular stress-raisers, Archive of Applied Mechanics 86 (2015) 375–401.

[19] G. Catalanotti, P. Camanho, A semi-analytical method to predict net-tension failure of mechanically fastened joints in composite laminates, Composites Science and Technology 76 (2013) 69–76.

[20] S. Timoshenko, J. N. Goodier, Theory of Elasticity, McGraw-Hill Book Company, Inc., 1951.

[21] M. H. Sadd, Elasticity: Theory, Applications, and Numerics - Second Edition, Elsevier Butterworth-Heinemann, 2005.

[22] J. H. Michell, On the direct determination of stress in an elastic solid with application to the theory of plates, Proceedings of the London Mathematical Society 31 (1899) 100–124.

[23] J. P. Waszczak, T. A. Cruse, Failure mode and strength prediction of anisotropic bolt bearing specimens, Journal of Composite Materials 5 (1971) 421–425.

[24] D. Leguillon, Strength or toughness? A criterion for crack onset at a notch, European Journal of Mechanics - A/Solids 21 (1) (2002) 61 – 72.